



UNIVERSITÀ DEGLI STUDI DI PADOVA

Dipartimento di Fisica e Astronomia “Galileo Galilei”

Corso di Laurea in Fisica

Tesi di Laurea

Numerical simulation of the secondary volume emission in a negative hydrogen ion beam

Relatore

Dr. Gianluigi Serianni

Correlatori

Dr. Pierluigi Veltri

Dr. Carlo Poggi

Laureando

Edoardo Spadetto

Anno Accademico 2018/2019

Abstract

ITER is an experiment to prove the possibility of obtaining energy from the nuclear fusion. In its heating system it needs negative ions accelerators and to obtain preliminary information about the beam optics and behaviour of these, numerical codes are used. In this thesis work one of these simulation codes, called IBSimu , has been adapted to simulate not only the primary beam optics, but also to take account of the possibility of reaction between accelerated particles and the background gas, and eventually track the reactions product. Moreover many simulation have been done, not really with the purpose to predict the behaviour of ELISE, the accelerator geometry used, but more to verify the proper operation of the developed code.

Contents

1	Introduction	3
1.1	Energetic Problem	3
1.2	Nuclear Fusion	3
1.3	ITER	4
1.4	ITER External Heating Systems	6
1.4.1	Neutral Beam Injectors	6
1.5	Beam Generation, Extraction, and Acceleration	7
1.6	Reactions	8
2	Modeling of the secondary particles related phenomena	10
2.1	Introduction to IBSimu	10
2.2	The Modified Algorithm	11
2.3	Monte Carlo Method	12
2.3.1	Monte Carlo Method Check	14
2.4	Space Charge Damping	19
3	Physical data behaviour under the variation of parameters	21
3.1	Step of interaction	21
3.1.1	Deflection Angle as function of the step of interaction	21
3.1.2	Divergence as function of the Step of Interaction	22
3.1.3	Currents as function of the Step of Interaction	23
3.1.4	Time as function of the Step of Interaction	25
3.1.5	Final Consideration for the Step of Interaction	25
3.2	Pressure of the background gas	27
3.2.1	Deflection as function of the Pressure Parameter	27
3.2.2	Divergence as function of the Pressure Parameter	28
3.2.3	Current as function of the Pressure Parameter	29
3.2.4	Test on the conservation of the current	32
3.2.5	Forecast on EG current	35

1 Introduction

1.1 Energetic Problem

By the end of the century the demand for energy is expected to triple due to the continue growth in population and due to the expansion of the industrial sector in developing countries. For this reasons scientists are focused in developing a new technology that would use nuclear fusion's reactions to produce energy. The advantages of a technology using this method are, in first place, the absence of emissions and refuses harmful for environment and second the paltry cost of the fuel.

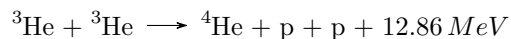
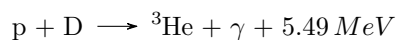
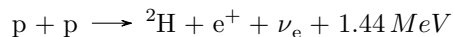
1.2 Nuclear Fusion

Nuclear fusion is a reaction in which two or more atomic nuclei are combined to form one different nucleus and other subatomic particles. The energy released by the reaction can be found using the Einstein's formula:

$$\Delta E = (\sum m_{r_i} - \sum m_{p_i})c^2 \quad (1)$$

Where m_{r_i} is i-th reagent's mass, m_{p_i} is the i-th product's mass and c the speed of light. This energy, named Q-value, could be positive or either negative depending if the energy is released or absorbed by the reaction.

Nuclear fusion reactions occur naturally in stars, for example in the Sun the main source of energy comes by the so called "p-p chain", a sequence of reactions that lead to the composition of a ${}^4\text{He}$ from two protons, in particular:



The first controlled nuclear fusion in laboratory was obtained by Mark Oliphant in 1932 but making it a source of energy is still a challenge for nowadays scientists.

1.3 ITER

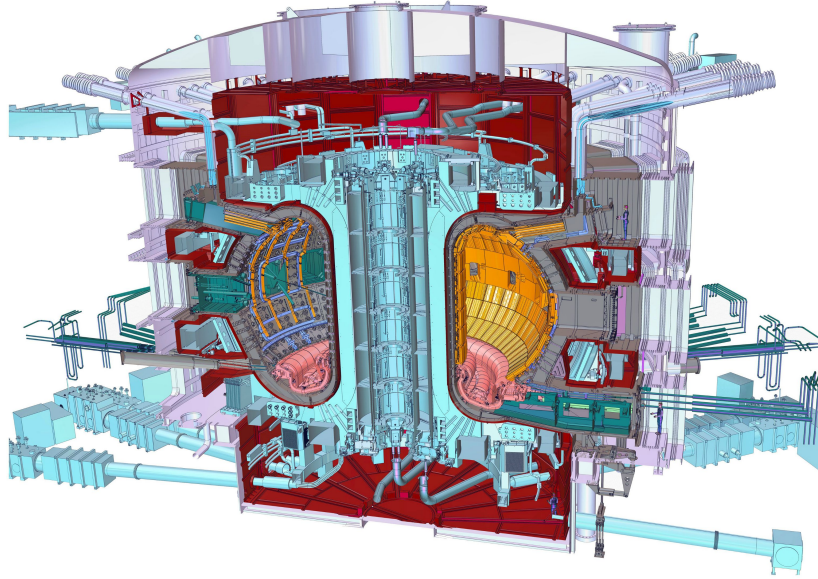
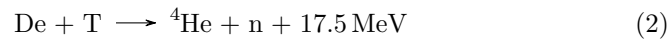


Figure 1: The ITER tokamak reactor

ITER acronym of International Thermonuclear Experimental Reactor is an international project to build a plasma reactor in which can occur a nuclear fusion reaction. To be specific ITER is a Tokamak, machine in which the plasma confinement is obtained through a toroidal and a poloidal magnetic field. The reaction decided for ITER is a Deuterium Tritium fusion:



The reason of this choice is because it is the easiest to reproduce in laboratory, and also the most efficient for energy production, with a ΔE (1) of 17.5 MeV . The project has born in 2006 from a collaboration between China, European Union, United States, India, Japan, Korea, and Russia, and its purpose is to show the possibility to obtain energy from nuclear fusion, because even if the reaction has a positive Q-value, reaching the condition of reaction is very expensive in terms of energy. In particular the goal is to obtain 500MW of power from an input of 50MW when the actual record is of 16MW with 24MW. ITER now is in construction at Cadarache in southern France, but its components are manufactured in many laboratories around the world.

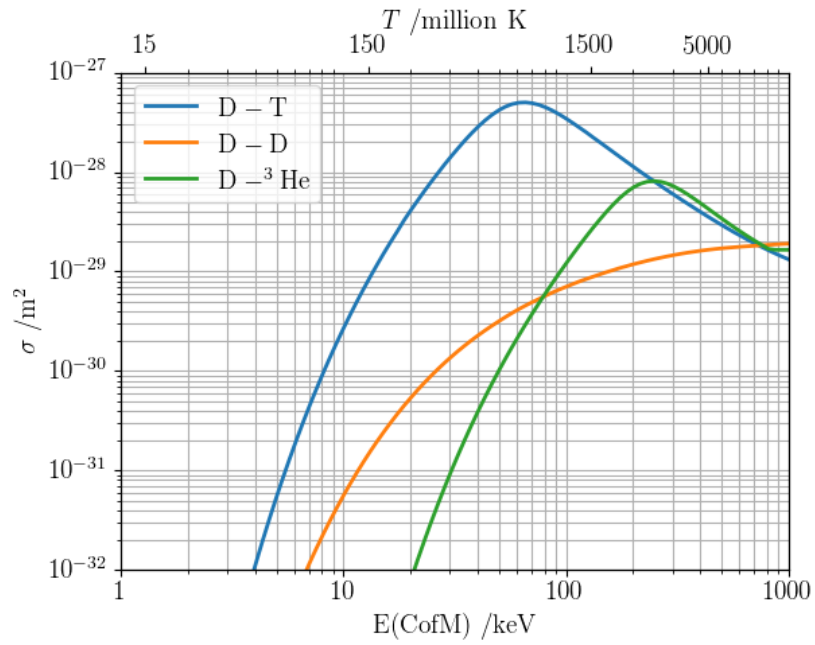


Figure 2: Graph showing cross sections(m^2) of $D - T$, $D - D$, and $D - ^3He$ nuclear fusion reactions as function of the energy of the reagents (keV).

1.4 ITER External Heating Systems

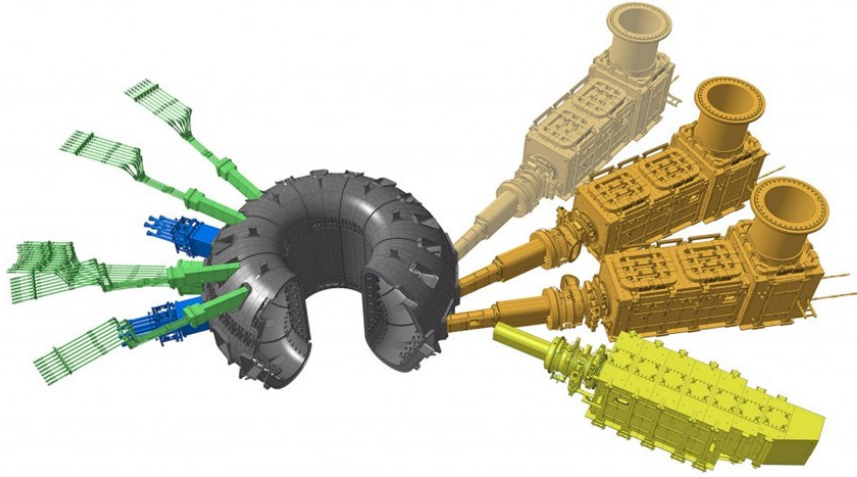


Figure 3: Neutral beam injection on the right in orange, sources of high-frequency electromagnetic waves—ion and electron cyclotron heating on the left in blue and green. The yellow machine on the left is the diagnostic of the beams.

To heat the plasma to reach temperatures that allow fusion reactions two main methods are used:

- Neutral Beam Injection
- Ion and Electron Cyclotron Resonant Heating

After arriving at such temperature researchers hope that the plasma will be able to keep itself that state using the energy of the ${}^4\text{He}$ nuclei produced in the reactions, in this case external generator are occasionally used or also be turned off.

1.4.1 Neutral Beam Injectors

Neutral Beam Injectors heat the plasma through a neutral particles beam that penetrates the plasma and its particles transfer energy in the collisions. For the ITER experiment it's planned the construction of two injectors with the possibility to install a third in the future, and these will be able to work for 3600 seconds with particle energies of 1MeV each, delivering a power of 16.5MW . NBI functioning can be divided in 3 main operations:

1. Beam Generation A ionized beam is extracted from a plasma with a system of electrodes at different potentials. In ITER's NBIs, there will be used H^-

ions generated through a volume process: $\text{H}_2 + e^- \rightarrow \text{H}^- + \text{H}$, and through two surface processes: $\text{H} + e^- \rightarrow \text{H}^-$ or $\text{H}^+ + 2e^- \rightarrow \text{H}^-$ that could be facilitated with a cesium layer on the internal surface of the source.

2. **Beam Extraction and Acceleration:** From the plasma the beam is extracted and also accelerated by a series of grids at different potentials. Between the first two grids usually there is a magnetic filter used to deflect the co-extracted electrons and that let pass the ions. Then the beam becomes more energetic and also changes its shape, in fact it can be made convergent or divergent as a function of the electrostatic potential and shape of the grids, even if the goal would be to have a perfectly cylindrical beam.
3. **Beam Neutralization:** The accelerated beam passes through a region of high pressure where the process of neutralization happens. The particles that remain charged are removed from the beam with a system of magnets.

1.5 Beam Generation, Extraction, and Acceleration

This thesis is mainly focused on the processes that happen in the generation and extraction phase in NBIs. The process of generation of the ions starts in specific chambers, called drivers, these can be made of Al_2O_3 or quartz and have a cylindrical shape. The ions that are created come from a plasma, ignited in the drivers through an RF coil and a starter filament. The filament inside of each driver is necessary due to the presence of another component, the Faraday Shield, this has vertical slits to allow the penetration of the magnetic field and protects the driver from plasma erosion, but it does not allow capacitive coupling necessary to start the plasma. The source area of ELISE, the facility simulated in this thesis, is about $0.87 \cdot 1\text{m}^2$, very similar to the width decided for the ITER sources but with a half height. An extraction system consists usually of three grids: PG (Plasma Grid), EG (Extraction Grid) and GG (Grounded Grid). To deflect electrons co-extracted with the ion beam is used a particular arrangement of permanent magnets, these deflect the electrons to the EG and let the ions pass. Due to a not perfect insulation of the source a significant amount of neutral gas can be found in the extraction system, this can interact with the accelerated particles and through chemical reactions other species of secondary particles are created.

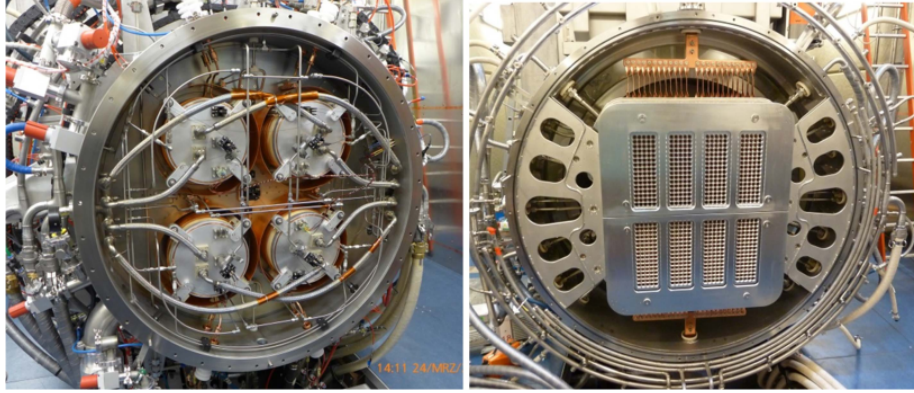
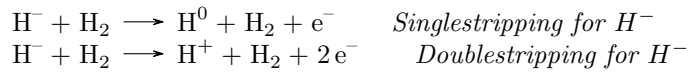


Figure 4: ELISE test facility, left: back side of ion source with 4 drivers (for operation in vacuum closed by a dome), right: view onto extraction system, showing the plasma grid and the bias plate (another grid before the PG to reduce the amount of co-extracted electrons); from the top the flexible copper conductors for the vertical PG current are visible, a corresponding connection is installed on the bottom side.

1.6 Reactions

Between all the reactions that can happen in an hydrogen based NBI it has been chosen to simulate only the most probable at range of energy of operation of the accelerator ($0 - 10^5 eV$). Now will follow the list of the considered reaction for each specie of possible reagent with the background gas.

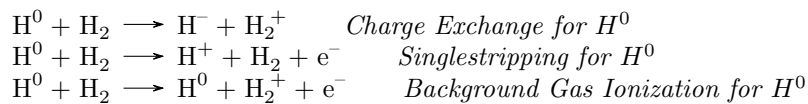
- For H^- ions have been considered two reactions.



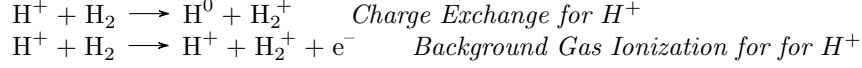
- For e^- have been considered two reactions.



- For H^0 have been considered three reactions.



- For H^+ ions have been considered two reactions.



- For H_2^+ have been considered only one reaction.



REACTANT	TYPE	PRODUCTS			INDEX
$H\cdot$	S	H^0 (F)	e^- (F)		1
$H\cdot$	S	H^+ (F)	e^- (F)	e^- (F)	2
e^-	BGI	$H_2^+(S)$	$H_2^+(S)$		3
e^-	DI	e^- (F)	H^+ (S)	$H^0(S)$ $e^-(S)$	4
H^0	CE	$H\cdot$ (F)	$H_2^+(S)$		5
H^0	S	$H^+(F)$	e^- (F)		6
H^0	BGI	H^0 (F)	e^- (F)	$H_2^+(S)$	7
H^+	CE	H^0 (F)	$H_2^+(S)$		8
H^+	BGI	H^0 (F)	e^- (S)	$H_2^+(S)$	9
H_2^+	CE	$H_2^+(S)$			10

Figure 5: Table showing all the reactions, respectively in the columns are specified the particle that reacts with the background gas, the type of reactions, the products with a specifier that let recognize if the product starts at rest is labeled as a slow particle (S) or if it keeps the velocity of the progenitor particle is labeled fast (F), and an index to identify a specific reaction.

The cross section of each reaction is calculated from fit parameters found in ALADDIN IAEA Database [Ref. 1] and in particular the two types of fits used are a polynomial fit of the logarithm of the cross section as function of the logarithm of the energy, and a Chebyshev polynomials fit always as function of the logarithm of the energy. In the IAEA Database these fit functions can be found in form of FORTRAN routines under the names of ALJAN1 and CHEB. In the program each reaction is only considered inside the energy limits parameters found in the database, outside this interval the cross section is considered null. Although for this problem of acceleration of H^- ions it has been decided to use these reactions, the program has been organized in a way that allows the

user to add or remove reactions or also simulate the interaction with another type of background gas.

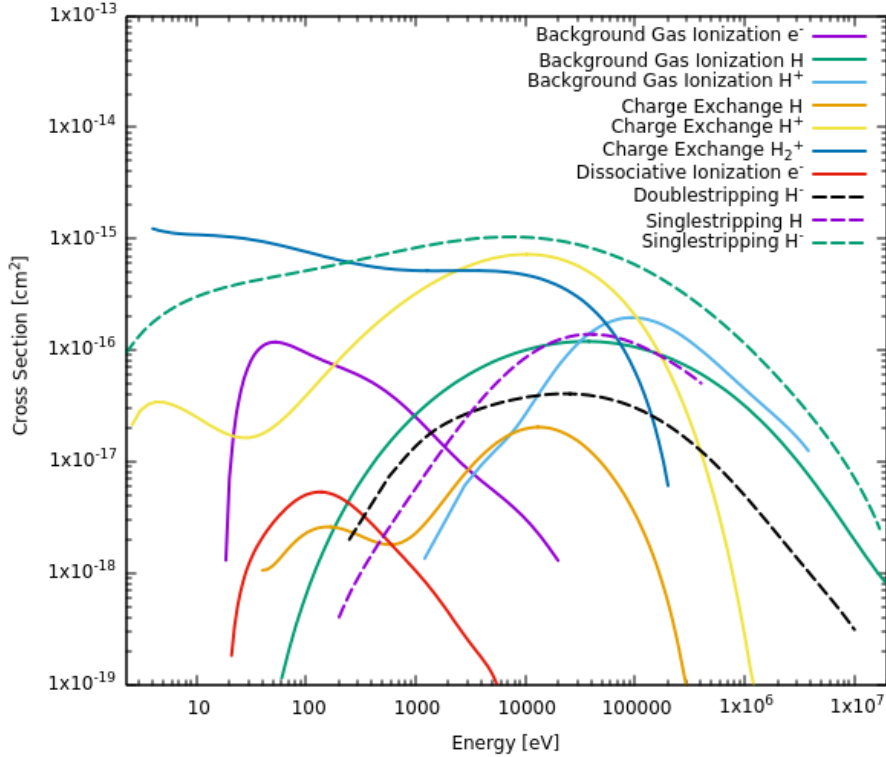


Figure 6: Cross sections of the different reactions as function of the energy of the impinging particle

2 Modeling of the secondary particles related phenomena

2.1 Introduction to IBSimu

IBSimu is a C++ library that allow to simulate the optic of an ion beam, this is under an open source license so it can be freely modified by the user. The purpose so was to write a code using these libraries to simulate the reactions processes exposed in the previous section. A standard simulation of IBSimu occurs in a discretized domain, the mesh, where it is possible to define the geometry of the electrodes, their electrostatic potential conditions and the magnetic field. The solids representing the electrodes can be uploaded through SLT/CAD files or defined as boolean functions. After this is necessary to define the particle

databases, objects that keep the information of every particle, in which will be defined the beam emitters. The code continues calculating the *Laplace equation* with a *finite difference method (FDM)* respecting the previous boundary conditions :

$$\nabla^2 V = 0 \quad (3)$$

Moreover it computes the electric field from the potential:

$$E = -\nabla V \quad (4)$$

and it starts iterating the particles through the mesh. The solution of the motion equations of the particles is obtained with a *Runge-Kutta* algorithm found in the GNU scientific library. During the iteration a space charge is deposited in the 8 nodes of every mesh cell where the particle has passed. This space charge is used to calculate the *Poisson Equation* :

$$\nabla^2 V = \frac{\rho}{\epsilon_0} \quad (5)$$

The process of iteration of the particles, space charge deposition and the calculation of the new electrostatic potential is repeated until a convergent solution is reached. The processes executed by the code are reported in the flux diagram in figure 7.

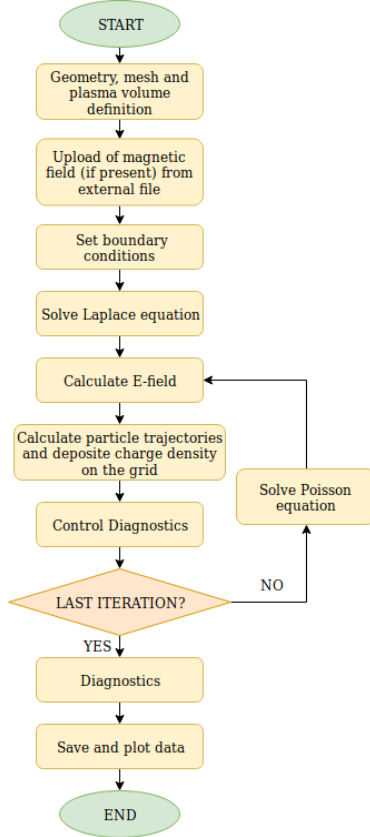


Figure 7: IBSIMU functioning flux diagram

2.2 The Modified Algorithm

To make possible the simulation of the reactions with the background gas the code has been modified with two

different processes added to the standard algorithm of IBSimu:

1. A Monte Carlo Method to simulate reactions
2. Space Charge Attenuation in convergence cycle

2.3 Monte Carlo Method

Precisely the reactions with the background gas are simulated with a Monte Carlo Method analogous to the one explained by *Fubiani et al.* in [Ref. 4]. In the simulation this part of the code operates after the convergence cycle of the electrostatic potential field, so, its purpose is to evaluate the behaviour of secondary particles in a field calculated only with the primaries but modified with a theoretical calculation on the H^- decay (space charge damping).

The process of simulation of the reactions works in parallel to an IB-Simu function that allows to step particles forward of a Δt . Due to the acceleration of the particles caused by the electric field this Δt can not be set as a fixed value but it has to be adapted to the velocity of the particles. This process of Δt recalculation happens each time before the particles are stepped forward, and it is meant to advance the fastest particle of a fixed Δz , called *step of interaction*, and decided in advance. In particular the form of the Δt is :

$$\Delta t = \frac{\Delta z}{v_{max}} \quad (6)$$

where v_{max} is speed of the fastest particle and Δz a fixed length comparable to unit of the mesh. It can happen that particles of the same kind, and so belonging to the same database, could have very different speeds, so an adequate Δt for the fastest ones could not let the other particle to advance of a reasonable length. In this case it is necessary to advance this database of particles for a greater number of steps than the others that do not have this issue. In this way the fastest ones can end their trajectory and after that the Δt will be no more influenced by their velocity, this because particles labeled as collided are not taken in account in the Δt calculation. This way also the other particles can continue their path and be simulated.

The Monte Carlo method evaluates first the probability that the impinging

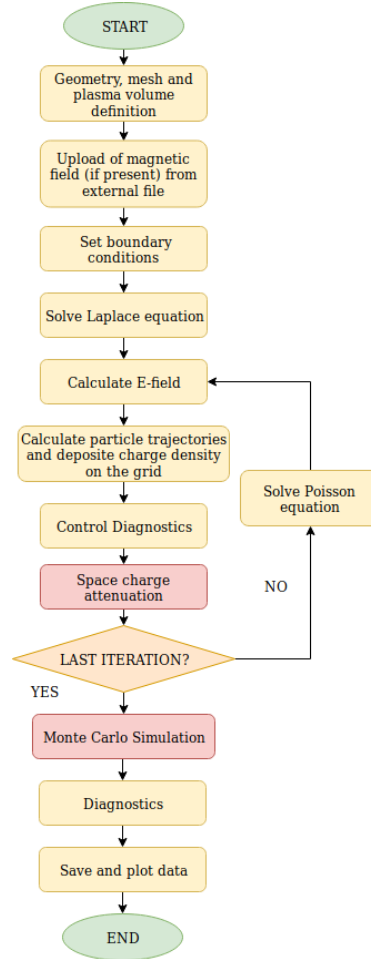


Figure 8: Diagram of the modified algorithm

ions would react in the last $\Delta z = v\Delta t$ interval they travelled as:

$$P(\Delta z) = 1 - e^{-n\sigma_{tot}v\Delta t} \quad (7)$$

where n is the density, σ_{tot} the sum of all the possible reactions' cross sections for the considered particle, and v , the speed at the end of this interval. This probability is then compared with a random number to check if the collision happened or not. If the collision happens the particle is labeled as collided and code has to calculate which of the possible processes happened. This is made by calculating the probability of each possible reactions as intervals of a unit. The limits of the i -th interval are:

$$\sum_{j=0}^{i-1} \frac{\sigma_j}{\sigma_{tot}}, \sum_{j=0}^i \frac{\sigma_j}{\sigma_{tot}} \quad (8)$$

where σ_j is the cross section of the j -th reaction. After this another random number from 0 to 1 is generated and depending on which interval contains it, the corresponding reaction is considered happened and the products are added to their specific database (Fig. 9). The products of a reactions are added with an initial position that is the last of the reagent particle, and they are differentiated according to whether they come from the projectile or from the H_2 target,

in the first case they are generated with the same speed of the reagent while in the second they are created steady.

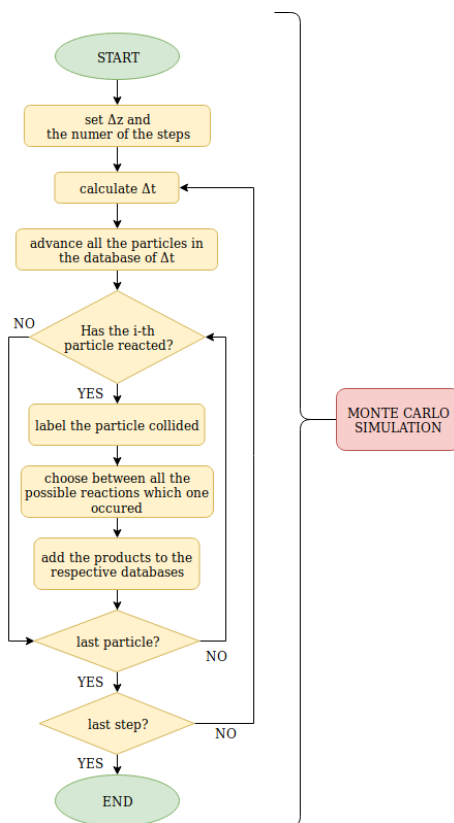
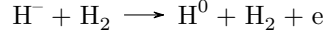


Figure 9: Diagram of the Monte Carlo Method

2.3.1 Monte Carlo Method Check

To control the correct functioning of this part of the code some tests have been made:

- The first test was an H^- beam that could have made only a single stripping reaction.



From now to identify a reaction, it will be used the indexes reported in figure 5, for example, σ_i will mean the cross section of the reaction with index i . For what regards cumulative cross sections of many reactions it would be expressed with more subscripts, for example: σ_{i-j-k} means the cumulative cross section of the i , j , and k reactions. This simulation has been made with $N_{0H^-} = 40000$ macro-particles, with a starting energy $E_A = 3 \cdot 10^4 eV$, in a constant pressure of $P = 0.3 Pa$ with no electric field and not considering the electrostatic interaction between particles. The density, calculated with the *Ideal Gas Law*:

$$p = nk_bT$$

So the parameters were:

$$\sigma_1 = 7.71261 \cdot 10^{-20} m^2 \quad n = 7.24638 \cdot 10^{19} m^{-3} \quad T = 300K$$

So knowing :

$$\begin{cases} dN_{H^-} = -N_{H^-}(z)\sigma_1 n dz \\ N_{H^-}(z=0) = N_{0H^-} \end{cases} \quad N_{H^-}(z) = N_{0H^-} e^{-\sigma_1 n z} = N_{0H^-} e^{-5.588z} \quad (9)$$

where $N_{H^-}(z)$ is the population of H^- ions and $N_{0H^-}(z)$ the initial population. Because the number of macro-particles in the simulation does not represent the physical parameter of the population of the beam it has been decided to normalize the functions as:

$$f(z) = \frac{N_{H^-}(z)}{N_{0H^-}} = e^{-5.588z} \quad (10)$$

This compared to the data resulted from the Monte Carlo simulation with a χ^2 test:

$$\tilde{\chi}^2 = \frac{1}{M} \sum_{i=0}^M \frac{(f_{H^-i} - f(z_i))^2}{f(z_i)^2} = 1.165 \cdot 10^{-4}$$

where f_{H^-i} is the observed data of the simulation at the z_i coordinate.

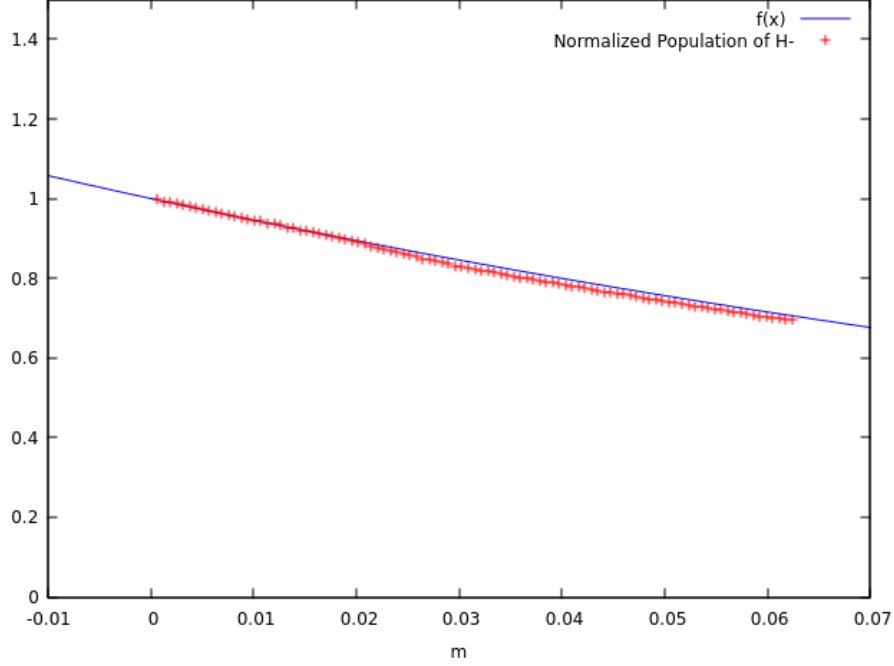


Figure 10: A comparison between the function $f(z)$ (10) and the respective data obtained from the simulation

- Then also the data from the H_0 particles generated from the single stripping reactions of the previous simulation, were analyzed. The energy of the H^0 is still $E_A = 3 \cdot 10^4$ because in the single stripping reaction they are generated with the same velocity of the H^- . Considering that an H_0 can make the reactions 5 , 6 and 7. the cumulative cross section is:

$$\sigma_{5-6-7} = 2.92397 \cdot 10^{-20} m^2$$

With the same density and same temperature as before. So knowing:

$$\begin{cases} dN_{H^0} = -N_{H^0}(z)\sigma_{5-6-7}ndz + N_{H^-}(z)\sigma_1ndz \\ N_{H^0}(z=0) = 0 \end{cases} \quad (11)$$

the law that regulates the population of H_0 is:

$$N_{H^0}(z) = N_{0H^-} \frac{\sigma_1}{\sigma_1 - \sigma_{5-6-7}} \cdot (e^{-\sigma_1 nz} - e^{-\sigma_{5-6-7} nz})$$

that, normalized as $\frac{N_{H^0}(z)}{N_{0H^-}}$, become:

$$g(z) = -1.6106 \cdot (e^{-5.5888z} - e^{-2.1188z}) \quad (12)$$

And so the comparison with a $\tilde{\chi}^2$ -test between the analytic and numerical results is:

$$\tilde{\chi}^2 = \frac{1}{M} \sum_{i=0}^M \frac{(f_{H^0_i} - g(z_i))^2}{g(z_i)^2} = 1.5 \cdot 10^{-2}$$

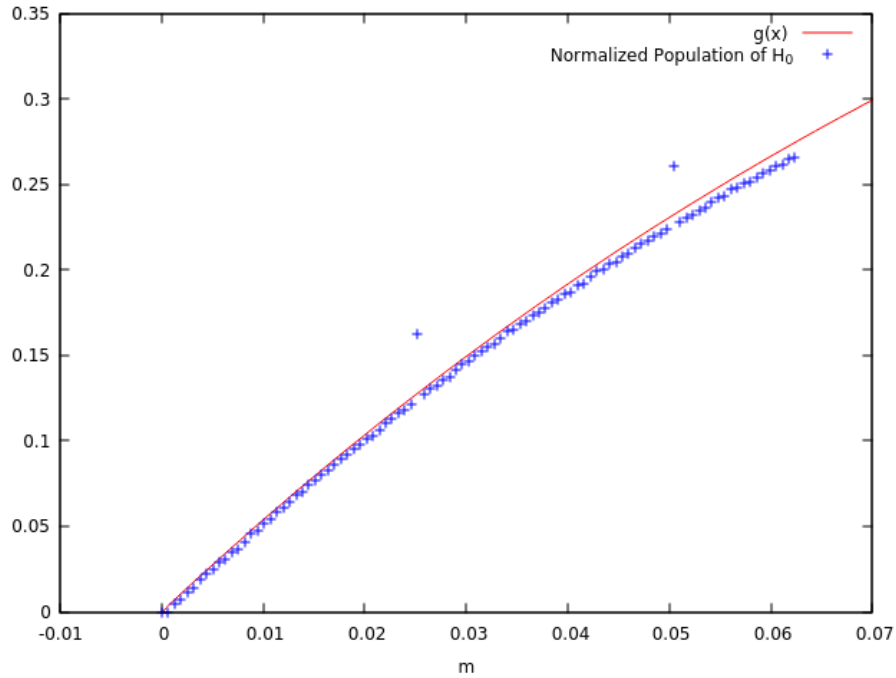


Figure 11: A comparison between the function $g(z)$ (12) and the normalized data of the simulation, the two points outside the line are caused by the coincidence between the diagnostic point and the limit of a cell mesh, this leads to instabilities in the results

- Finally the code has been used for a more realistic case, the simulation occurred in the ELISE accelerator geometry (Fig. 13) and to save computational time it has been limited only to one of the 640 apertures embedded in the electrodes. Hence the energy of the particles and so their cross section is not constant along the z axis, in fact electrostatic potential of the grids was: $\Phi_{pg} = 0V$, $\Phi_{eg} = 5000V$, and $\Phi_{gg} = 31000V$. The pressure

profile had been approximated constant in correspondence of the grids and linearly decreasing between them. This profile was calculated relying on the results of a dedicated software for the study of diffusion of neutral gas in molecular flow regime [Ref. 10]. The three levels were respectively at: $0.3Pa$, $0.1Pa$ and $0.01Pa$.

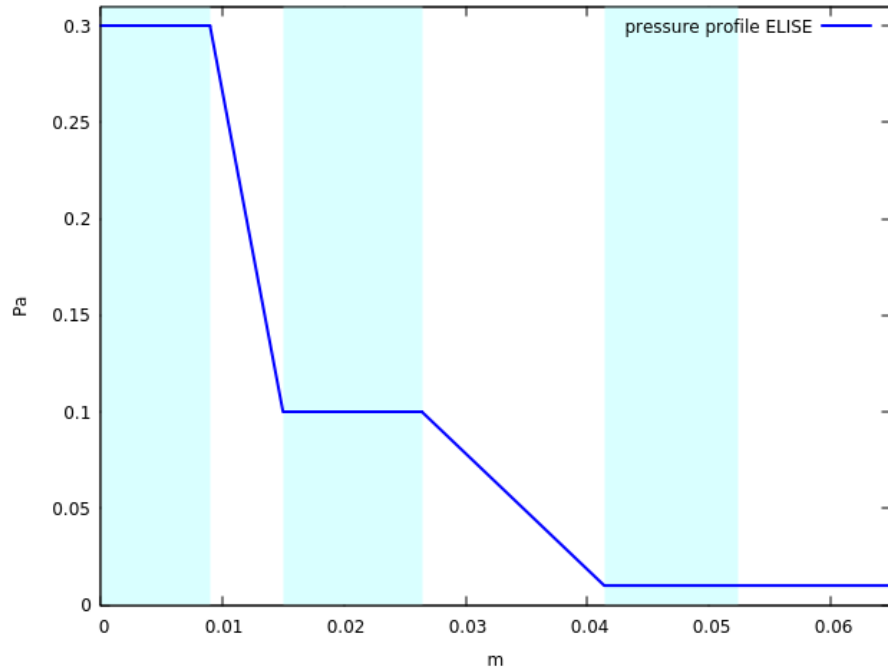


Figure 12: ELISE pressure profile along the z axis , in cyan are evidenced the grid locations: from the left to the right PG (Plasma Grid), EG (Extraction Grid), and GG (Grounded Grid)

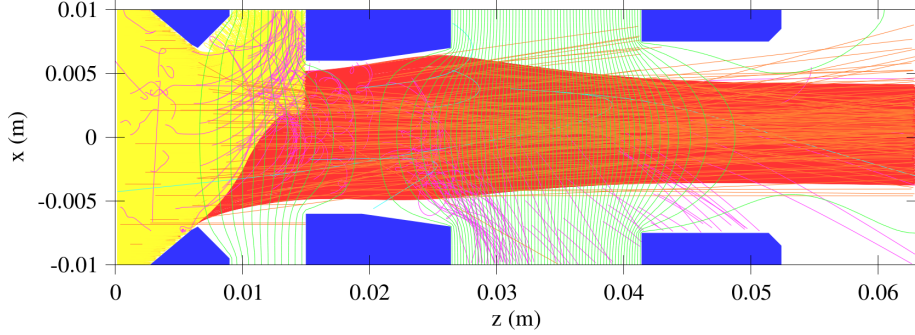


Figure 13: Elise accelerator geometry in a single beam configuration. The blue regions are the grids, and respectively from the left PG (Plasma Grid , $V_{pg} = 0V$) , EG (Extraction Grid , $V_{eg} = 5 \cdot 10^3V$) and GG (Grounded Grid , $V_{gg} = 3.1 \cdot 10^4V$). It represent also the beam in a typical simulation $j_{H^-} = 150 \frac{A}{m^2}$ and $j_{e^-} = 150 \frac{A}{m^2}$. In yellow and purple are evidenced primary and secondary electrons respectively, in cyan H^+ ions and red H^- , and in orange the H^0

For this simulation only two reactions for H^- have been enabled, namely single stripping and double stripping reactions (Fig. 5). Since in this configuration the electric field derives from the combination of the electrode potentials and from the Coulomb's interaction between particles, to compute the solution of the exponential beam attenuation equation, numerical methods have been used. The first operation to do was to evaluate the energy, and so the cross section, as functions of the z coordinate. The energy gets calculated on the coordinates $x = 0$ and $y = 0$, this choice is justified by the fact that radially the electrostatic potential varies of a minimal quantity compared to the variation along the z axis (on the order of $10V$) (Fig. 13).

$$E(z) = q[V(0, 0, z) - V_0(0, 0, 0)] + E_0 \quad (13)$$

$$\sigma_{1-2} = \sigma_{1-2}(E(z))$$

where q is the charge of an H^- particle, $V(0, 0, z)$ the electrostatic potential on the axis z (keeping $x, y = 0$), E_0 the starting energy of a particle and $E(z)$ the energy as function of the z coordinate.

From the beam attenuation equation:

$$dN_{H^-} = -N_{H^-} \cdot \sigma_{1-2}(z)n(z)$$

and the expected solution was:

$$N_{H^-} = N_{0H^-} \cdot \exp\left[-\int_{z_0}^z \sigma_{1-2}(\tilde{z})n(\tilde{z})d\tilde{z}\right] \quad (14)$$

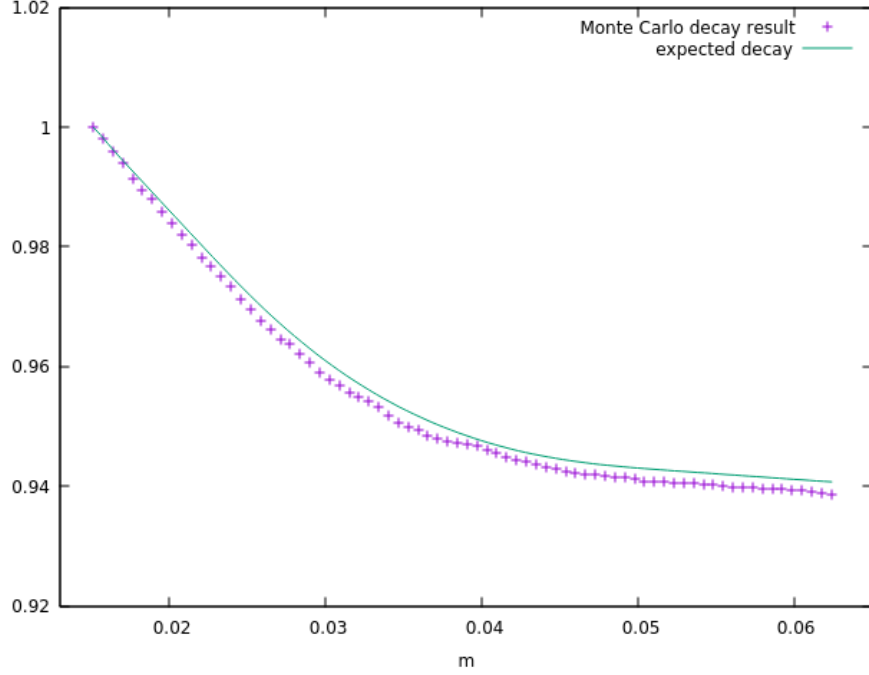


Figure 14: Plot of the expected population normalized to $N_{H^-}(z = 0.01512)$ and the observed H^- one in ELISE geometry. $z = 0.01512m$ has been chosen because it is the first data after the EG so not influenced by primary electrons that are extracted just before that grid (Fig. 13)

This graph (Fig. 14) shows the tendency of the population obtained with the Monte Carlo method to be slightly lower than the expected one. This is due to the fact that for the evaluation of the analytical decay it has been used a 1D profile for the potential, namely $V=V(0,0,z)$, while the real one, used in the Monte Carlo approach, is actually tri-dimensional. Anyway to show that the expected data are compatible with the observed ones it has been made a χ^2 - *test*:

$$\tilde{\chi}^2 = \frac{1}{N} \cdot \sum_{i=0}^N \frac{(f_{oi} - f_{ei})^2}{f_{ei}^2} = 2,32 \cdot 10^{-4}$$

From the three tests above it is possible to see that the Monte Carlo Method respects the analytic results from the exponential beam attenuation equation.

2.4 Space Charge Damping

The Monte Carlo Method that has been discussed before does not work during the electrostatic potential convergence cycle so in order to take in account the

beam current attenuation along the axis it has been decided to rescale the space charge distribution $\rho_0(x, y, z)$ as:

$$\rho'(x, y, z) = \rho_0(x, y, z) \cdot \exp\left[-\int_{z_0}^z \sigma_{1-2}(\tilde{z}) \cdot n(\tilde{z}) \cdot d\tilde{z}\right]$$

Where ρ' is the new space charge, ρ_0 the standard space charge calculated by the IBSimu function during one iteration, z_0 the starting z point of the beam, σ_{1-2} the cumulative cross section for all the H^- -reactions and n the numerical density. To compute this sum obviously n and σ_{1-2} are needed. The density n is calculated from pressure data, with the *Ideal Gas Law*. The energy is computed knowing the electrostatic potential and the starting energy of the particle.

$$E(z) = q(V(z) - V(z_0)) + E_0$$

It has been decided to only use the cross sections of the H^- reactions in the decay factor, this because primary electrons are deflected in the first part of the accelerator from the magnetic field. Secondary electrons created in the interactions with the background gas are faster than H^- so they do not affect much space charge. For example an electron with the same energy as an ion would deposit in a mesh cell a space charge of approximately:

$$\rho_e = \frac{j_e}{v_e} = \frac{j_e \sqrt{m_e}}{\sqrt{2E}} \quad \rho_i = \frac{j_i}{v_i} = \frac{j_i \sqrt{m_i}}{\sqrt{2E}}$$

$$\frac{\rho_e}{\rho_i} = \frac{j_e \sqrt{m_e}}{j_i \sqrt{m_i}}$$

that for $j_i \approx j_e$ is $\frac{\rho_e}{\rho_i} \approx \frac{1}{40}$. The condition of comparable current densities is easily achieved in H^- accelerators where the source surface underwent a cesium deposition treatment, otherwise e^- linked space charge could become determinant in the extraction phase, where these particles are not deflected yet.

For what regards the other secondary particles considered in the Monte Carlo method, such H_2^+ and H^+ their density is much lower than H^- due to the fact they are only generated through reactions with a marginal probability, otherwise H_0 they obviously do not have charge. A verification of the correct functioning of this process can be found in the figure 14, in fact the way how the factor of damping gets calculated is the same numerical integral computed in the third test made for the Monte Carlo method.

3 Physical data behaviour under the variation of parameters

In this chapter, first, it will be presented a study about the Step of Interaction, the only computational parameter that can be changed in the code without modifying the physics of the problem. So the purpose of this study was to find the best value of this parameter, that allows a not too long simulation, and also one that would give coherent results respect to the IBSimu standard iterator. In the second part the results of simulations, varying the background gas pressure, will be exposed. Hence these simulations study the behaviour of the code varying a physical parameter, the pressure, so in different configuration of the accelerator. In correspondence of these test will also be analyzed some aspects of the current results that did not represent exactly our expectation.

3.1 Step of interaction

The step of interaction is the maximal length that a particle could travel before its reaction got checked, and it coincides with the $\Delta z = v\Delta t$ of the previous section (7). This parameter is chosen by the user and it is expected that for smaller values respect to the mesh unit, it would lead to more accurate simulations, instead bigger values would lead to instabilities in the results. It will follow a study to evidence the behaviour of the simulation's physical parameters under the variation of the step of interaction.

3.1.1 Deflection Angle as function of the step of interaction

The deflection angle is the mean angle of deflection of the beam. and it is defined as:

$$\overline{\theta}_s = \frac{\sum_{n=1}^N \arctan\left(\frac{v_{s-i}}{v_{z-i}}\right)}{N} = \frac{\sum_{n=1}^N \theta_i}{N} \quad (15)$$

where v_{s-i} is the velocity of the i -th particle along the s axis, and N the total number of particles. From the graph (Fig. 15) it is possible to see that the X value of the deflection is slightly negative due to the magnetic field, and for bigger values of the step of interaction shows the expected deviation from the predicted value. The Y values instead have much smaller deviations and they seem not to be influenced by the step of interaction. So, for this action restricted only to X value, the variation of the deflection angle could be only a consequence of the action of the magnetic field on the beam, and not really a parameter influenced by the step of interaction.

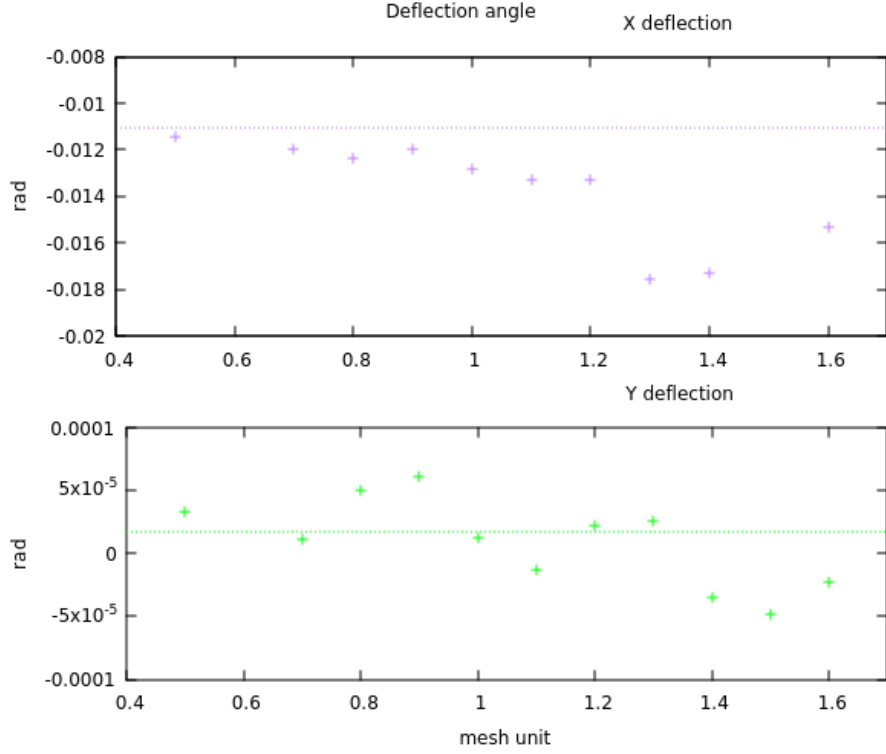


Figure 15: Deflection of H^- particles along the X axis above and under it the Y deflection, the dashed lines represent the expected values in the case without the possibility of interaction with the background gas (using the standard IBSimu code)

3.1.2 Divergence as function of the Step of Interaction

The divergence is the standard deviation of the angle of deflection with a chosen axis:

$$\sigma_{\theta-s} = \sqrt{\frac{\sum_{n=1}^N (\theta_i - \bar{\theta}_s)^2 i_i}{I_{tot}}} \quad (16)$$

where v_{s-i} means the component of the velocity of the i -th particle parallel to the s axis, N the total number of particles, $\bar{\theta}_s$ the mean angle, $\sigma_{\theta-s}$ the divergence on the s axis, i_i and I_{tot} are respectively the currents of the i -th particle and the sum of all the currents carried by the particles.

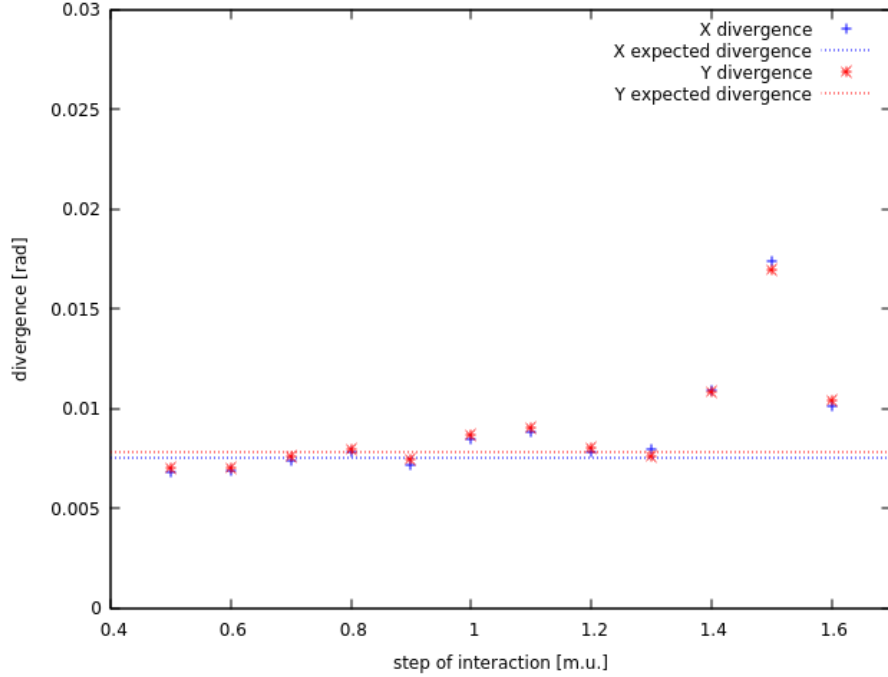


Figure 16: Graph showing the divergence of H^- particles along the axis X and Y as function of the step of interaction (expressed in mesh unit), the dashed lines represent the expected values of the divergences calculated without the possibility of interaction

From the graph (Fig. 16) emerge that for smaller steps of interaction the divergence has a certain stability that keeps its values around the expected one. Anyway there is not a perfect approach of the divergences of the lowest steps of interaction to the expected one. This probably happens because the IBSimu standard iterator has the feature of adapting its length of advancement to the variation of the electrostatic potential to optimize the work done by the CPU. Instead the iterator used in the Monte Carlo simulation simply calculates the time of advancement as $\Delta t = \frac{\Delta z}{v_{max}}$ where Δz is the step of interaction and v_{max} the speed of the fastest particle.

3.1.3 Currents as function of the Step of Interaction

In this section it is exposed a study that shows the correlation between the outgoing current, and the currents at EG (Extractions Grid) and GG (Grounded Grid). From the graph it is possible to verify the stability for all the currents in correspondence of lower values of the step of interaction. Anyway it is clear that it is not possible that the one showed in figure 17 is really the current colliding on the EG. This evidences a problem in the C++ routine used to diagnostic the

current to the grids. In fact to measure the aforesaid currents the algorithm sums all the currents carried by the particles that have last trajectory point inside the solid. This condition does not take in account many particles, knowing that most of the primary electrons should collide to the extraction grid. This problem can be caused by the particles that does not collide on the simulation solid but on the side boundary of the mesh. A possible solution to this could be implementing an algorithm that once a particle collide with a side, it gets put back from the opposite one (particle mirroring), anyway in the next section it will be proposed an alternative to interpret these data. Moreover the currents in the graph, despite they do not give a physical information, they are useful to show the stability and the correct functioning of the program, so to find the best value for the step of interaction.

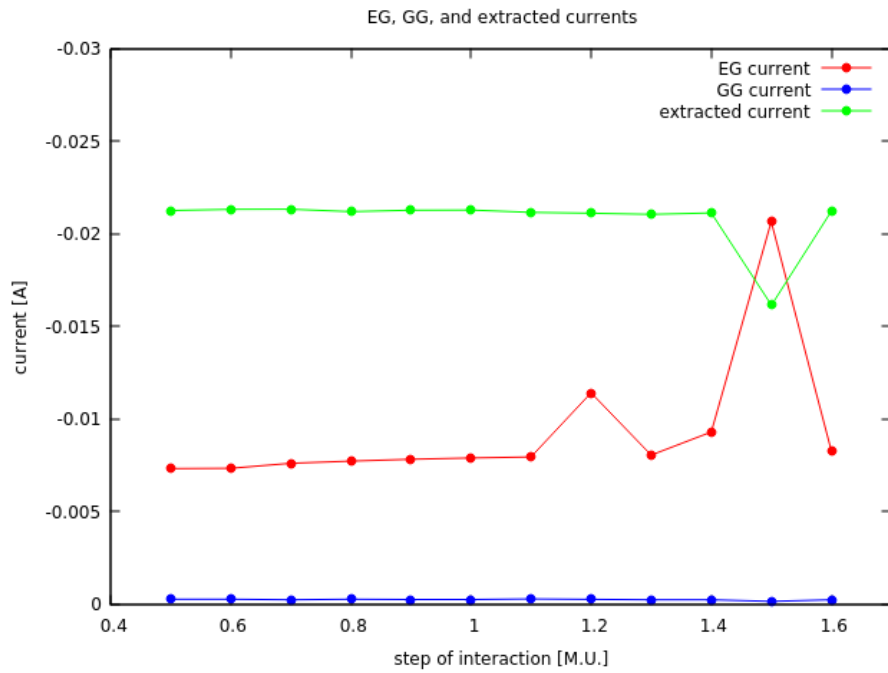


Figure 17: Graph showing the currents at EG (Extraction Grid), GG (Ground Grid) and the extracted one as function of the step of interaction expressed in M.U. length of the side of a mesh cell.

3.1.4 Time as function of the Step of Interaction

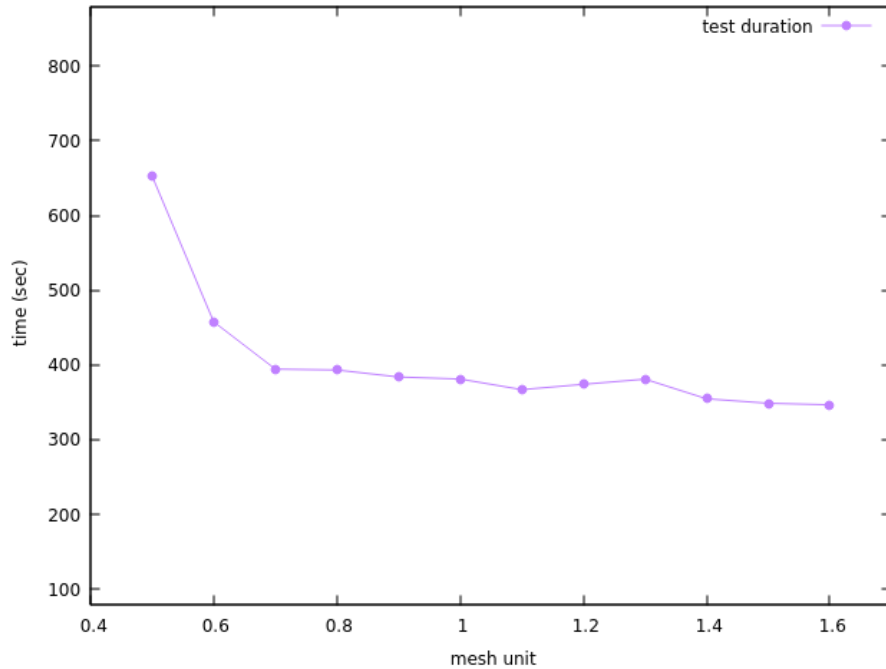


Figure 18: Duration of a simulation in the ELISE geometry as function of the step of interaction (expressed in mesh unit length)

The duration of a simulation decreases for bigger values of the step of interaction. This happens because the beam end its trajectory in less steps and so the number of times that the interaction of particles, with the background gas is checked, decreases.

3.1.5 Final Consideration for the Step of Interaction

From a look to the graphs of the standard deviations of the deflections and of the divergences, (Fig. 19) it is possible to confirm the forecast on the stability for lower values of the step of interaction. The instabilities for the X deflections are shown from the $1.4m.u.$ value, otherwise as said above, the Y deflection does not seem to vary tion of the step of interaction. The divergences show a growth in correspondance of the $1.3m.u.$ value. Moreover the analysis of the duration of simulation (Fig. 18) does not show big variations in the time used after the $0.7m.u.$ values. From these evidences it has been decided for the next simulation to use a step of interaction of $\Delta z = 0.8m.u.$: a good compromise between being precise and a not too slow simulation.

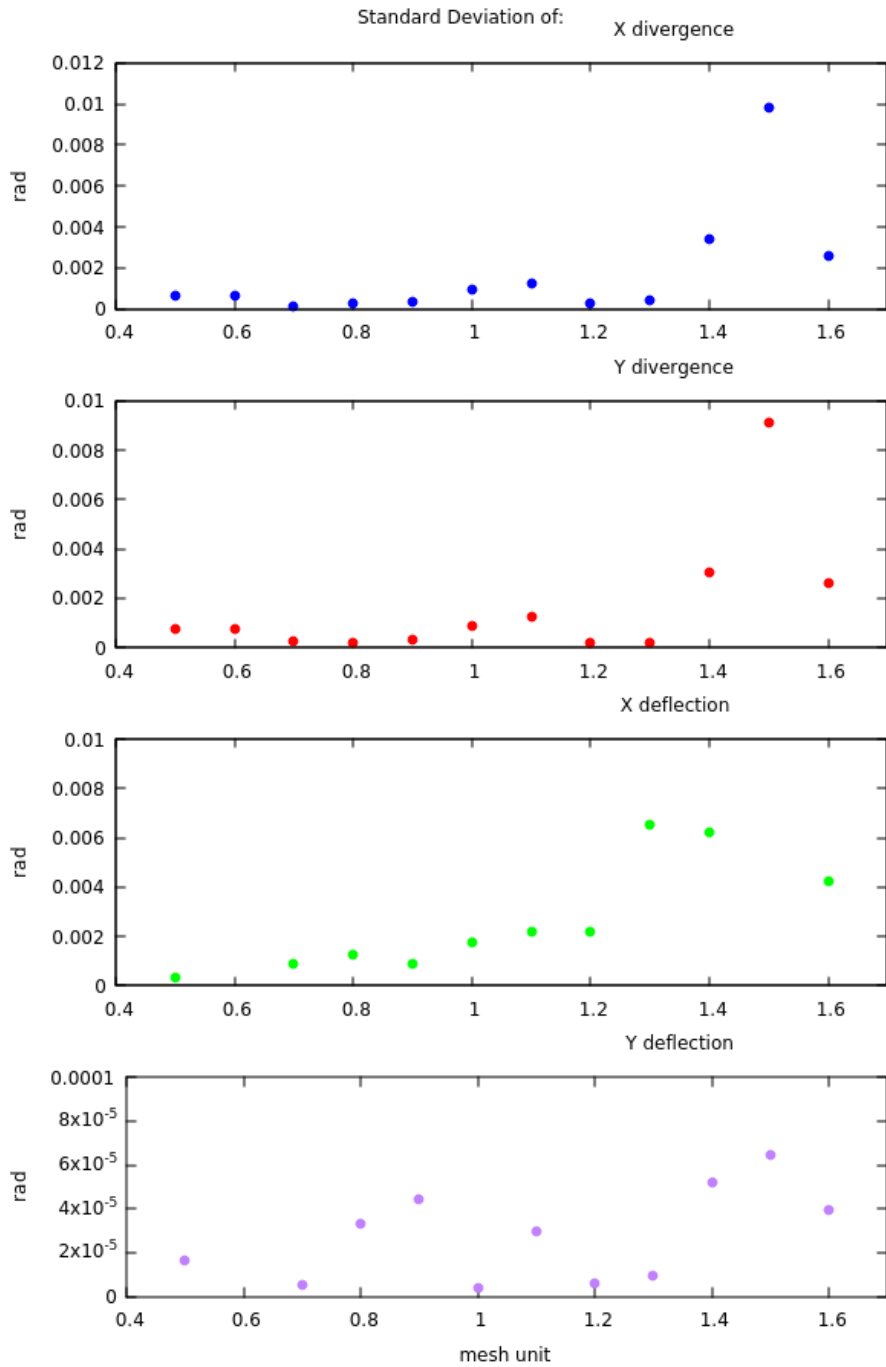


Figure 19: Standard Deviation of X and Y divergences and deflection angles respect to the expected values

3.2 Pressure of the background gas

After the optimization of the value of the step of interaction it has been decided to evaluate the behaviour of the simulation under variations in the pressure profile. These variations consisted in the multiplication of the pressure profile by a parameter: called in the following paragraphs *pressure parameter* or *pressure factor*. Using a ladder shape profile it becomes:

Pressure Parameter	PG (Pa)	EG (Pa)	GG (Pa)
0,000	0,000	0,000	0,000
0,500	0,150	0,050	0,005
1,000	0,300	0,100	0,010
1,500	0,450	0,150	0,015
2,000	0,600	0,200	0,020
2,500	0,750	0,250	0,025
3,000	0,900	0,300	0,030
3,500	1,050	0,350	0,035
4,000	1,200	0,400	0,040

Figure 20: The pressure profile is considered constant at the grids and linearly decreasing between them. In the figure are reported the values of pressure at the grids in correspondence of the pressure parameter.

The study made with the variation of pressure analyzed the same parameters of the previous section: divergence, deflection angle and the currents.

3.2.1 Deflection as function of the Pressure Parameter

The variation of the deflection angle under different pressure profiles seems caused by the magnetic field. In fact the Y deflection, not influenced by the magnetic filter, does not show variations, otherwise the X deflection grows slightly under the pressure variations.

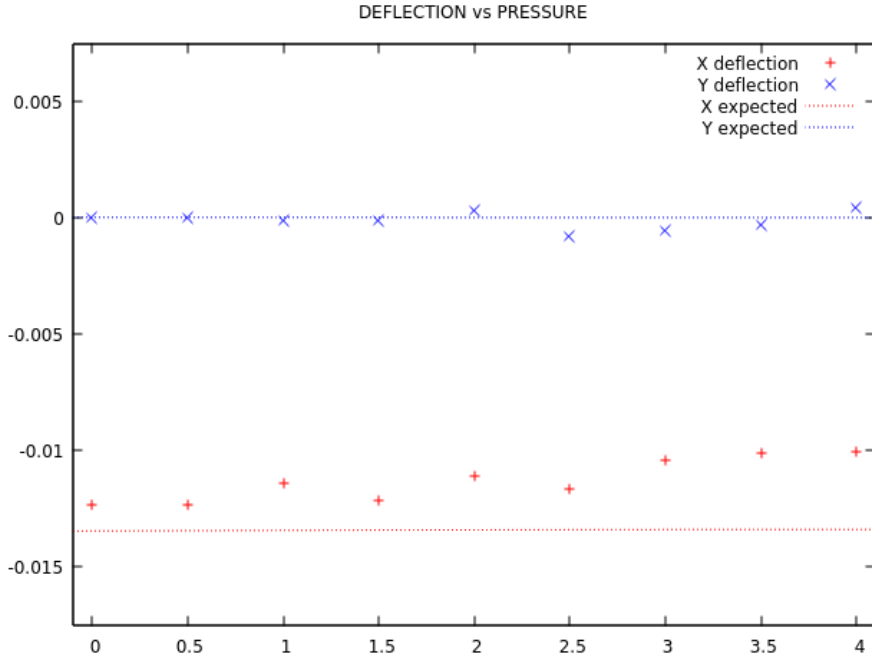


Figure 21: X and Y deflection (rad) varying the pressure parameter. The dashed lines are the X and Y deflection angles for the primaries

3.2.2 Divergence as function of the Pressure Parameter

The divergences of the H^- along the X and Y axis grows as function of the pressure parameter (Fig. 22) whether they are iterated with the standard IBSimu code or with the function in the Monte Carlo method. This can be explained by the fact that higher pressure leads to more reactions, this decreases the H^- population and so it destabilizes the optic. Moreover it is possible to see that the divergences calculated with the two different iterators grows with different slopes. This happens because the space charge damping factor is calculated only with the electrostatic potential on the z axis (13) while the Monte Carlo method evaluates the probability of interaction for every step of advancement. Another cause of this issue could be the fact that the Monte Carlo method iterates the particle in a different way than the standard IBSimu iterator so also this can lead to discrepancies in the results, that were expected to be equal.

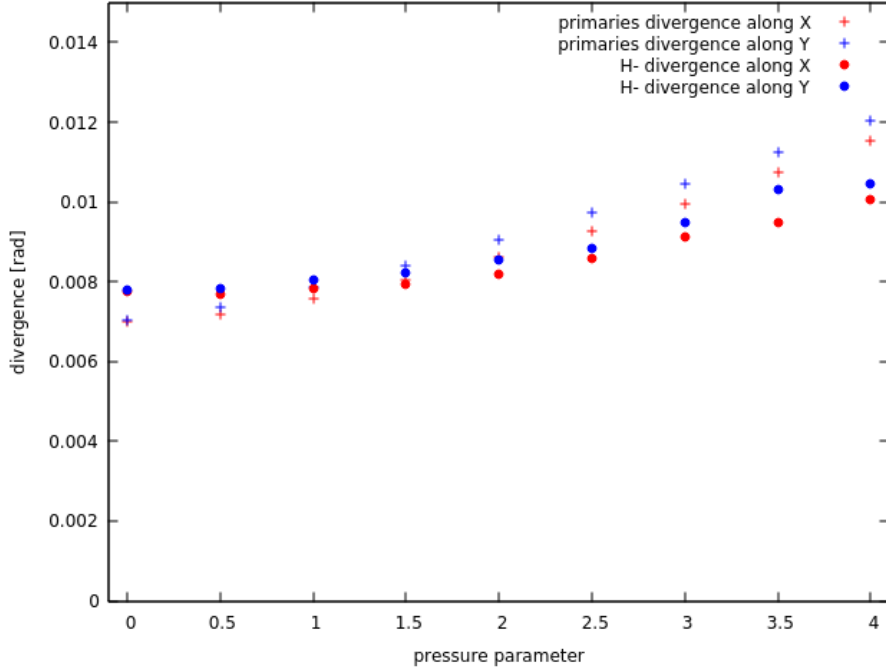


Figure 22: X and Y divergence (rad) varying the pressure parameter of primaries using standard IBSimu iterator with space charge damping (the crosses) , and the results of divergence with the Monte Carlo method (the points).

3.2.3 Current as function of the Pressure Parameter

The last study regarded the behaviour of the currents under pressure variations. In particular the currents on the grids PG(Plasma Grids), EG (Extraction Grid), and GG (Grounded Grid) have been analyzed. The incoming ($z = 0.0068m$, PG edge) and exiting current($z = 0.06m$, after GG) , and the ones exiting from the mesh domain from the sides. These lasts physically are colliding to the grids or passing to another beam hole. The graphs below shows the incoming and extracted current (Fig. 23). The incoming one as expected is stable as function of the pressure parameter. In fact before exiting the PG the electric field is suppressed to simulate plasma conditions, this along with the fact that for low energy the reactions can not happen, it leads to stability. Anyway the value in the simulation is slightly lower than the expected one.

$$I_{in-exp} = j_{tot}\pi r^2 = 4.618 \cdot 10^{-2} A$$

where I_{in-exp} is the total expected incoming current (at $z = 0.0068m$), j_{tot} the total current density and r (r at $z = 0.0068m$) the lowest radius value in the PG. The value of I_{in-exp} although is different from the ones from the simulation it is still compatible with them, in fact they differ only by the 2%. For what

regards the exiting current its behaviour coincides with the expected one, its values increase with the pressure parameter, and this is caused by the fact that more particles react and not arrive to the end of the accelerator.

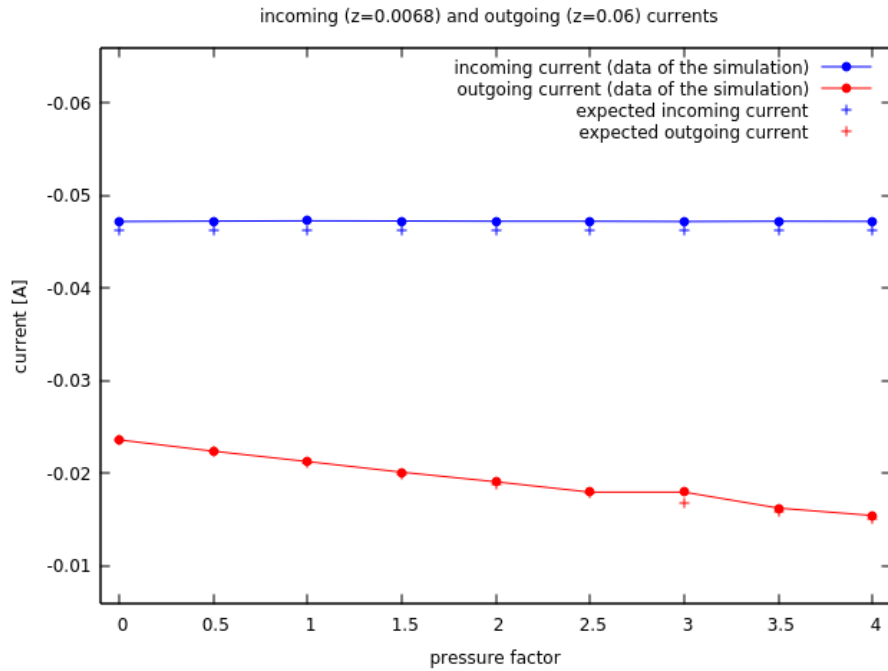


Figure 23: In the graph is shown the current entering the volume after the point of the smallest radius of the plasma grid ($z = 0.0068m, I_{in}$), and the current exiting after the grounded grid ($z = 0.06m, I_{out}$), all as function of the pressure parameter. The crosses are the expected values calculated using the space charge damping (14).

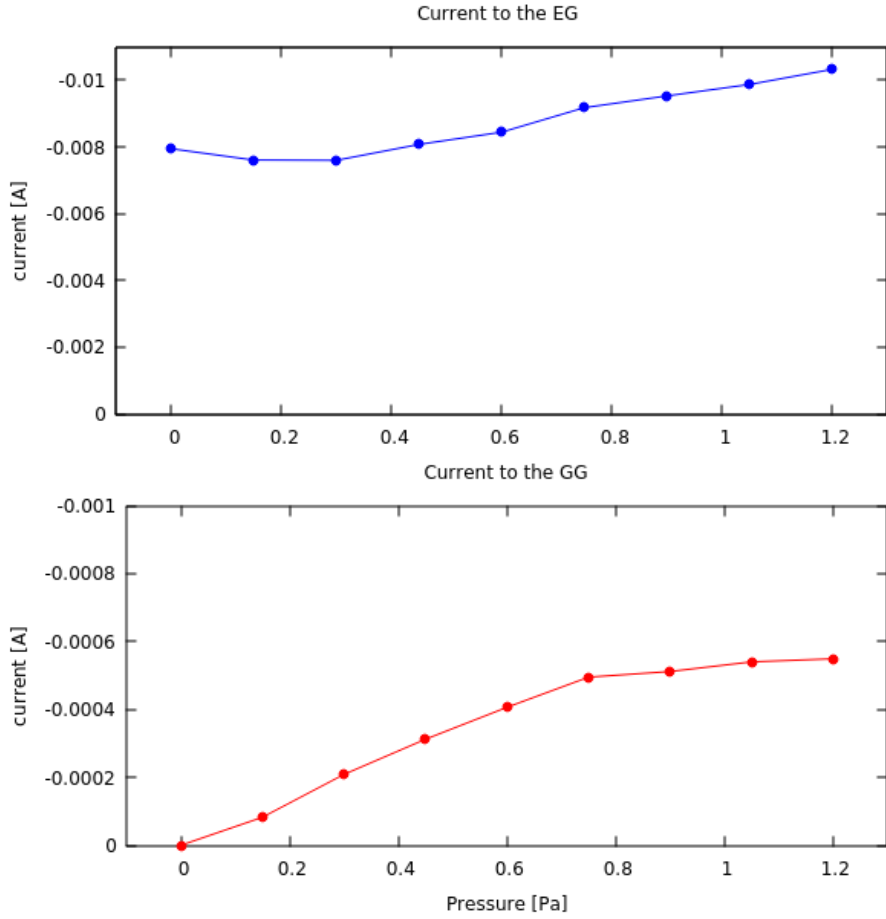


Figure 24: Currents colliding to the EG and GG as function of the pressure at the source. Computed as the current carried by the particles that have their last trajectory point inside the boolean function that represent the grids.

In the graph above (Fig. 24) it is shown that the current colliding on the EG is rising for the lowest values of the pressure parameter and then starts decreasing. The part of reduction (0.3 Pa / 1.2 Pa) of the current happens due to the fact that the predominant reactions of single stripping and double stripping generate secondary electrons that sum with the primaries and then they are extracted together. The part of growth (0.0 Pa / 0.3 Pa) was not expected and its explanation is not linked to the physics of the Monte Carlo method. The problem is caused by an imprecision in the diagnostics of the current. For the iterator that has been used, IBSimu does not allow to use its data analysis functions, so as explained in the figure 24 the current to the grids has been estimated as the sum of all the currents carried by the particles which have their last trajectory point inside the boolean function that represent the

solid. This way of proceeding can evidence the stability of the program and its parameters but does not allow a physical forecast of the currents. This is obvious thinking that the magnetic filter should divert most of the electrons to the EG but the current on this grid is only a small part of the incoming current carried by all electrons (half of the incoming current, Fig. 23). To be sure that this problem was caused really by the diagnostics and not by errors in the program it has been decided to make a test on the conservation of the current in a chosen volume.

3.2.4 Test on the conservation of the current

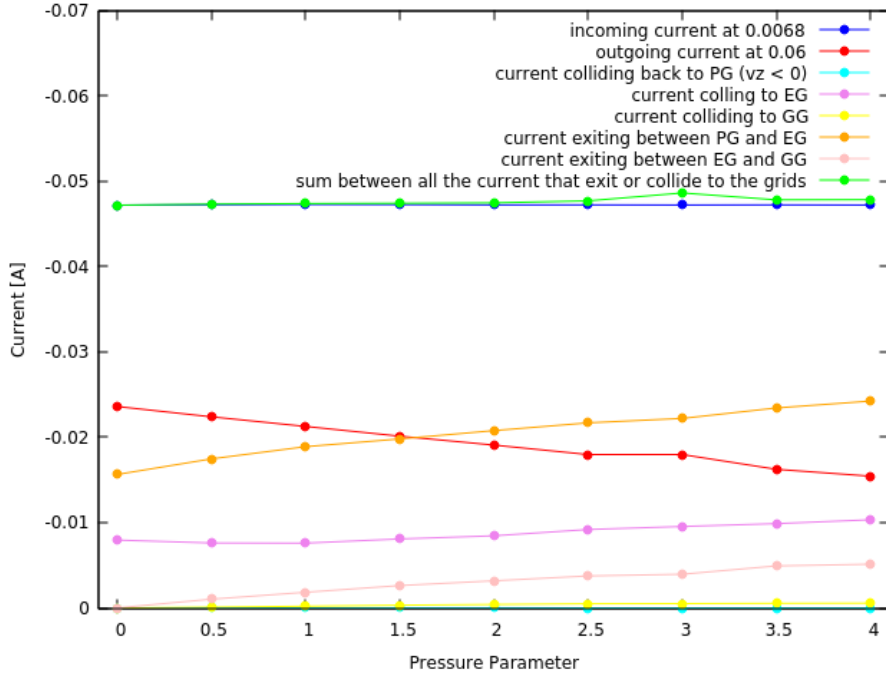


Figure 25: Summary graph of all the currents as function of the pressure parameter. in blue I_{in} , in red I_{out} , in cyan $I_{PG-back}$, in violet I_{EG} , in yellow I_{GG} , in orange $I_{sides-PG-EG}$ (19), in pink $I_{sides-EG-GG} = I_{sides} - I_{sides-PG-EG}$ (17), and the sum of all these currents except for I_{in} in green ($I_{green} = I_{tot} - I_{in}$ (18)).

To make this test the chosen volume was delimited by the planes $z = 0.0068m$ and $z = 0.06m$, by a part of the Plasma Grid, by the Extraction and the Grounded Grid, and then also by the mesh boundaries. To compute the incoming (I_{in}) and outgoing currents (I_{out}) along the z axis, it has been used

a simple IBSimu diagnostics that check how many particles trajectories intersected a plane, and the results were exactly the ones exposed in (Fig. 23). For what regards the currents colliding with the grids, as before it has been decided to sum all the current carried by the particles that have their last trajectory point inside a specific solid. Instead, to calculate the current exiting on the sides it has not been possible to calculate it as the sum of all the current carried by the particles which have their last trajectory point outside the domain of the mesh, this would have led to not taking in account many macro-particles and so a great amount of current. To measure this current it has been decided to sum the current of every particles labeled collided in the volume between the edge of the plasma grid ($z = 0.0068m$) and the last point of the extraction grid ($z = 0.6m$), this current will be called I_{dec} . This method has the defect to count the portion of particles that simply made a reaction inside this region as if they have gone outside the mesh through the sides. Hence, to partially correct this source of error it has been chosen to subtract from it the current of all the H^- ions which reacted in this volume ($I_{H_{dec}^-}$), this current has been calculated with the (14), in particular :

$$I_{H_{dec}^-} = I_{0H^-} \cdot (e^{-\int_{z_0}^{0.0068} \sigma_{1-2}(\bar{z})n(\bar{z})d\bar{z}} - e^{-\int_{z_0}^{0.06} \sigma_{1-2}(\bar{z})n(\bar{z})d\bar{z}}) \quad (17)$$

$$I_{sides} = I_{dec} - I_{H_{dec}^-}$$

Where I_{0H^-} (at $z = 0.0068$) is the incoming current of H^- , σ_{1-2} the cumulative cross section following the notation in figure 5, and I_{sides} the current exiting from the mesh domain. Obviously the correction made this way will not be complete in fact also the other species of particles (e^- , H^+ , H_2^+) that carry current can decay and these are not counted in the correction, but the biggest part of the reaction is made by the H^- .

The graph in figure 25 represents I_{tot} : the difference between the incoming current in the volume delimited by the mesh, the grids and the planes at the z coordinates $z = 0.0068m$ and $z = 0.06m$.

$$I_{tot} = I_{in} - I_{out} - I_{PG-back} - I_{EG} - I_{GG} - I_{sides} \quad (18)$$

and

$$s = 100 \cdot \frac{I_{tot}}{I_{in}}$$

I_{tot} is the sum between the incoming and exiting current in the volume, that should be zero, I_{in} is the incoming current at $z = 0.0068m$, I_{out} the exiting current at $z = 0.06m$, $I_{PG-back}$ the current colliding to the PG with negative speed, I_{EG} , I_{GG} the current to the two grids, and I_{sides} is the one showed in the (17). The condition $I_{tot} = 0$ is verified only for $p.p. = 0$ (p.p = pressure parameter) and after it it grows. This is caused by the choice of the diagnostic

of the current to the sides explained before. Increasing the pressure promotes more reactions and the one of the e^- , H^+ and H_2^+ happening in the considered volume are not taken in account in the correction of the (16), causing the growth as function of the pressure parameter. Moreover the second graph shows the percentage discrepancy over the incoming current, and it grows almost exactly as the graph above.

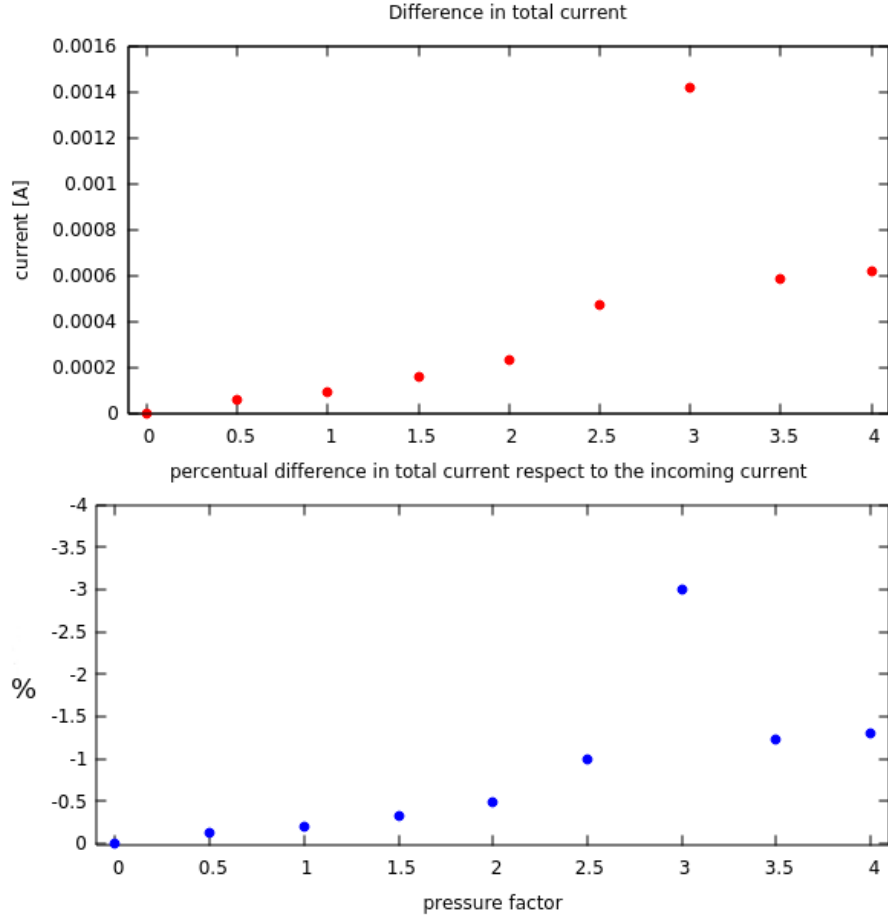


Figure 26: Test to check the conservation of the current, chosen a volume the incoming and exiting current have to give zero sum. The volume considered is the one from $z = 0.0068m$ and $z = 0.06m$, the sides of the mesh and the grids. In the first graph it is shown I_{tot} (17), while in the second s the percentual fraction of I_{tot} over I_{in} .

3.2.5 Forecast on EG current

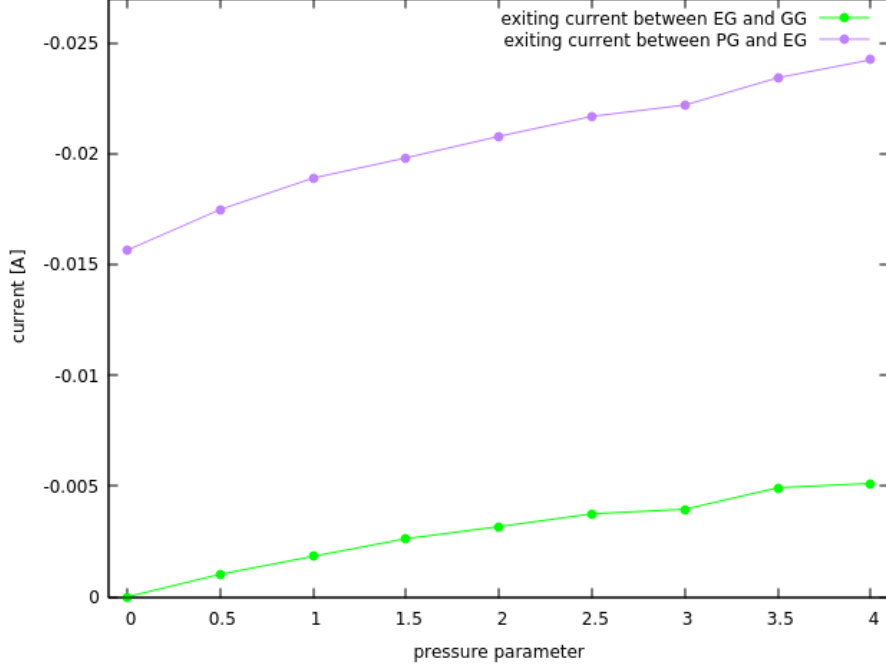


Figure 27: In the graph is shown the current escaping between PG and EG ($I_{corr-EG-PG}$) in purple, and second the one exiting between EG and GG in green, all as function of the pressure parameter.

Despite its evident limits this diagnostic of the current exiting by the sides helped to forecast the real EG current (I_{EG-r}):

$$I_{EG-r} = I_{EG} + I_{sides-PG-EG} \quad (19)$$

where $I_{sides-PG-EG}$ is :

$$I_{sides-PG-EG} = I_{dec-PG-EG} - I_{corr-EG-PG}$$

$I_{dec-PG-EG}$ is the sum of all the current carried by the particles labeled collided between the coordinates $z = 0.0068m$ (edge of the PG) and $z = 0.0264m$ (last point of the EG). $I_{corr-EG-PG}$ a similar correction to the one at (17) but made only between $z = 0.0068m$ and $z = 0.0264m$.

$$I_{corr-EG-PG} = I_{0H-} \cdot (e^{-\int_{z_0}^{0.0068} \sigma_{1-2}(\tilde{z})n(\tilde{z})d\tilde{z}} - e^{-\int_{z_0}^{0.0264} \sigma_{1-2}(\tilde{z})n(\tilde{z})d\tilde{z}})$$

For the GG this evaluation has not been done in first place because the currents on the boundary between EG and GG is lower, so more sensitive to errors, and second there is a greater distance between the two grids that suggests more complicated trajectories of the particles (it is more probable that a particle travels to another beam between these two grids than between PG and EG).

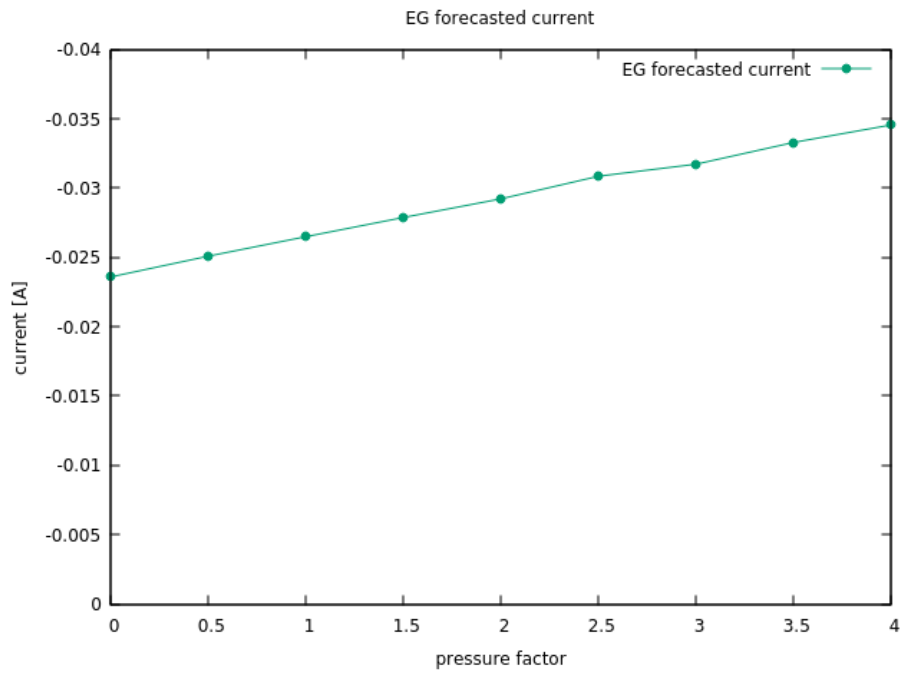


Figure 28: Forecast on the EG current (I_{EG-r}) as function of the pressure parameter

Conclusions

In this thesis the purpose was to develop a code able to take in account volume reaction in an H^- accelerated beam. The program has been modified in a way that makes it modular and lets to change easily the type of reactions considered in the beam, this makes it suitable for different types of accelerator that not exclusively accelerate H^- but also other ions, either negative or positive. For what regards its functioning the program showed itself to be stable and overall it behaved as predicted. For what regards the simulation we realized, they gave results coherent with the physical analysis of the problem, so the next step in its use should be the comparison of simulations with experimental data and check if the results are effectively more accurate than the ones of a standard IBSimu simulation. In future a way to improve the program could be the development of: a less intricate diagnostic system for the currents, able to track effectively every macro-particle trajectory and collision with boundaries and grids; or the adaptation of the standard IBSimu diagnostic to the Monte Carlo simulation. This improvement would not be really a necessity because also the current analysis used in 4.2.4 and 4.2.5 gave precise results, but it would be certainly more elegant to use only the data of the particle trajectories and not also a theoretical calculation in the diagnostics.

References

1. Official Site of ALADDIN Database, <https://www-amdis.iaea.org/ALADDIN/>
2. R. Callegari, "Studio dell'ottica di un fascio di ioni negativi e sua interazione con il gas di fondo", Tesi di Laurea, Università degli Studi di Padova, Dipartimento di Fisica e Astronomia "Galileo Galilei", 2018.
3. L. Fortunato, "Appunti di Fisica Nucleare", GEDI Gruppo Editoriale S.p.A, 2018.
4. G. Fubiani, H. P. L. de Esch, A. Simonin and R. S. Hemsworth, "Modeling of secondary emission processes in the negative ion based electrostatic accelerator of the International Thermonuclear Experimental Reactor", Phys. Rev. ST Accel. Beams 11, 014202, 2008.
5. B. Heinemann, U. Fantz, W. Kraus, L. Schiesko, C. Wimmer, D. Wunderlich, F. Bonomo, M. Frösche, R. Nocentini and R. Riedl, Towards large and powerful radio frequency driven negative ion sources for fusion , New Journal of Physics, Volume 19, January 2017
6. Official Site of IBSimu, <http://ibsimu.sourceforge.net/>.
7. Official Site of ITER , <https://www.iter.org/>.
8. T. Kalvas, "Development and use of computational tool for modelling negative hydrogen ion source extraction systems", Academic Dissertation for the Degree of Doctor of Philosophy, University of Jyväskylä, Department of Physics Research Report No. 10/2013, 2013.
9. A. Ludovici, "Study of an alternative extraction electrode for particle accelerator of NIO1 experiment", Tesi di Laurea, Università degli Studi di Padova, Dipartimento di Fisica e Astronomia "Galileo Galilei", 2017.
10. E. Sartori, P. Veltri. AVOCADO: A numerical code to calculate gas pressure distribution. Vacuum, 90(1), 80 - 88, 2013.